JACS
JOURNAL OF THE AMERICAN CHEMICAL SOCIETY

Article

pubs.acs.org/JACS

A Real-Time Surface Enhanced Raman Spectroscopy Study of Plasmonic Photothermal Cell Death Using Targeted Gold Nanoparticles

Mena Aioub and Mostafa A. El-Sayed*

Laser Dynamics Laboratory, School of Chemistry and Biochemistry, Georgia Institute of Technology, Atlanta, Georgia 30332-0400, United States

Supporting Information

ABSTRACT: Plasmonic nanoparticles are increasingly utilized in biomedical applications including imaging, diagnostics, drug delivery, and plasmonic photothermal therapy (PPT). PPT involves the rapid conversion of light into heat by plasmonic nanoparticles targeted to a tumor, causing hyperthermia-induced cell death. These nanoparticles can be passively targeted utilizing the enhanced permeability and retention effect, or actively targeted using proteins, peptides, or other small molecules. Here, we report the use of actively targeted spherical gold nanoparticles (AuNPs), both to induce PPT cell death, and to monitor the associated molecular changes through time-dependent surface enhanced Raman spectroscopy within a single cell. We monitored these changes in real-time and found that heat generated from the aggregated nanoparticles absorbing near-infrared (NIR) laser light of sufficient powers caused modifications in the protein and lipid structures within the cell and ultimately led to cell death. The same molecular changes were observed using different nanoparticle sizes and laser intensities, indicating the consistency of the molecular changes throughout PPT-induced cell death from actively targeted AuNPs. We also confirmed these observations by comparing them to reference spectra obtained by cell death induced by oven heating at 100 °C. The ability to monitor PPT-induced cell death in real-time will help understand the changes on a molecular level and offers us a basis to understand the molecular mechanisms involved in photothermal cancer cell death.

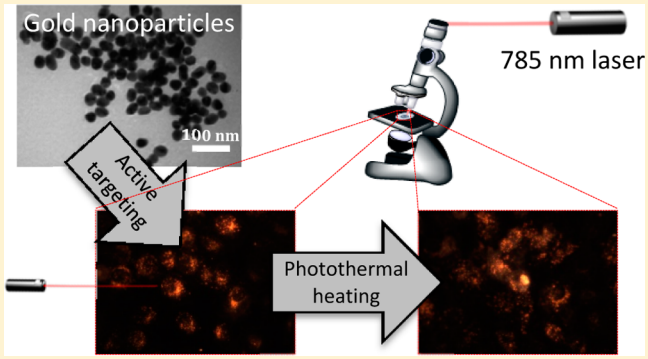

INTRODUCTION

The use of nanoparticles in biomedical applications has increased tremendously in recent years due to their biologically relevant size and the unique chemical, physical, and optical properties that arise on the nanoscale. Metallic nanoparticles have been heavily used in particular, due to the growing ease of their colloidal synthetic strategies, precise control over their size and shape, facile surface chemistry, and tunable optical properties.[1−5] Gold nanoparticles (AuNPs) exhibit these properties, along with low inherent toxicity, an essential requirement for biological applications.[6] They also display intense optical properties arising from their localized surface plasmon resonance (LSPR).[7] The LSPR arises from the coherent oscillation of electrons in the conduction band, in resonance with light of a particular frequency. The observed LSPR peak depends on the dielectric function of the metal nanoparticle and surrounding media, as well as the size and shape of the nanoparticle.[7,8] Therefore, the LSPR can easily be tuned for biological applications by adjusting the size and shape of the nanoparticles to control the observed wavelength and relative scattering/absorption properties.[8,9] This has led to the widespread use of AuNPs in cellular imaging (including both surface enhanced Raman scattering (SERS) for molecular fingerprinting and Rayleigh scattering for traditional imaging),[10,11] drug delivery/photodynamic therapy,[12−14] and plasmonic photothermal therapy (PPT).[15,16]

PPT is a promising cancer treatment where plasmonic nanoparticles rapidly convert NIR light to heat through the nonradiative relaxation of the excited LSPR through electron−electron, electron−phonon, and phonon−phonon collisions. These interactions generate an intense heating of the gold nanoparticle, leading to the hyperthermia-induced death of cells in close proximity to the nanoparticles.[9,15,17] Therefore, PPT relies on the accumulation of plasmonic nanoparticles in or around the cells of interest, which can be achieved through passive- or active-targeting.[18] AuNPs can be passively targeted to tumors through the enhanced permeability and retention (EPR) effect, which occurs due to the abnormal vasculature that results from tumor angiogenesis and results in the accumulation of nanoparticles and small molecules at the tumor site.[19] Nanoparticles can also be actively targeted to cancer cells using proteins, peptides, or small molecules, such as antiepidermal growth factor receptor or herceptin proteins, or

Received: October 20, 2015
Published: January 8, 2016

DOI: 10.1021/jacs.5b10997
J. Am. Chem. Soc. 2016, 138, 1258−1264

RGD peptides, which target overexpressed receptors on the cancer cell surface.[20] Significant research efforts have gone into characterizing cell death resulting from PPT treatment, and investigating specific proteins and signaling molecules, as well as the mechanisms underlying cell death (i.e., apoptosis or necrosis).[15,17,21,22] However, there have been many literature reports of both apoptotic[17,21] and necrotic[21,23−26] cell death resulting from PPT. These conflicting reports are most likely due to differences in the nanoparticle targeting (passive or active), physical properties (e.g., size, shape, absorption cross section, etc.) that dictate the absorption cross section, spectral overlap between the plasmon band and the laser used for PPT, and the intensity and duration of the laser exposure.

In the present work, we exploit the enhanced optical properties of AuNPs, namely, their strong absorption properties to induce PPT cell death, and their intense scattering to monitor the molecular changes that occur in real-time using SERS. While Raman scattering is a relatively old technique, the advent of enhanced Raman spectroscopies, such as SERS, has resulted in incredible enhancement factors of up to 10^{14}, making single molecule and single cell spectroscopies achievable.[27,28] Here, we have used actively targeted AuNPs and SERS to study PPT-induced cell death in real-time, as a function of both nanoparticle concentration and laser intensity. Because SERS enhancement is only observed in the AuNP microenvironment, we are able to follow the molecular changes that occur around the nanoparticles as heat is generated in real-time. We found a minimum threshold of laser intensity/nanoparticle concentration, below which heat dissipation outpaces heat generation and no cell death is observed. When above this threshold, the heat generated causes perturbations to lipid and protein structure, ultimately resulting in cell death. Increasing laser intensity leads to more rapid cell death, but the same biochemical changes are observed.

EXPERIMENTAL SECTION

Materials. Tetrachloroauric acid trihydrate ($HAuCl_4 \cdot 3H_2O$) and trisodium citrate were purchased from Sigma-Aldrich. Methoxy-poly(ethylene glycol)-thiol (mPEG-SH, MW 5000) was obtained from Laysan Bio, Inc. Custom RGD (RGDRGDRGDRGDPGC) and NLS (CGGGPKKKRKVGG) peptides were purchased from GenScript, Inc. Dulbecco's phosphate buffered saline (PBS), Dulbecco's modified Eagle's medium (DMEM), antibiotic solution, fetal bovine serum (FBS), 0.25% trypsin/2.2 mM EDTA, and propidium iodide (PI) were purchased from VWR. Annexin-V binding buffer was obtained from Invitrogen, Inc., and Annexin-V FITC was purchased from Biolegend.

Instrumentation. Transmission electron microscope (TEM) images were taken using a JEOL 100CX-2 microscope. Average nanoparticle particle diameter was measured using ImageJ software. UV−vis spectra were collected using an Ocean Optics HR4000CG-UV-NIR spectrometer. Dark-field images and SERS spectra were collected using a Renishaw InVia Raman microscope coupled with a Leica optical microscope and 785 nm diode Raman excitation laser. Flow cytometry experiments were performed using a BD LSR II Flow Cytometer (BD Biosciences).

Gold Nanoparticle Synthesis and Functionalization. Citrate-capped gold nanoparticles (AuNPs) were prepared following the Turkevich/Frens citrate reduction technique.[29,30] A 100 mL aqueous solution of 0.60 mM chloroauric acid was heated with stirring. Just before the solution reached boiling, 1 mL of 90 mM sodium citrate was added. Stirring and heating were discontinued, and the solution was allowed to cool to room temperature when a red-wine color was observed.

The citrate stabilized AuNPs were first cleaned by centrifugation at 4000× *g* for 15 min and redispersed in deionized (DI) water. The AuNPs were then conjugated with PEG to increase stability, enhance biocompatibility, and prevent nonspecific interactions in physiological environments.[20] A 1.0 mM solution of mPEG-SH in DI water was added to achieve a ∼20% surface coverage. The PEG-AuNP solution was shaken at room temperature overnight and unbound ligands removed by centrifugation (12,000× *g*, 7 min). PEG-AuNPs were again dispersed in DI water, followed by conjugation with a 1:10 ratio of RGD and NLS peptides to fill remaining surface sites. The AuNPs were centrifuged (12 000× *g*, 7 min) to remove unbound peptides and dispersed in DI water to yield nuclear targeted gold nanoparticles (NT-AuNPs).

Cell Culture. Human oral squamous carcinoma (HSC-3) cells, an epithelial cell line expressing $\alpha\beta$ integrins on the cellular membrane,[31] were used as our cancer model. The cells were cultured in DMEM supplemented with 10% v/v FBS and 1% v/v antibiotic. Cell cultures were maintained in a 5% CO_2 atmosphere in a humidified 37 °C incubator.

SERS Measurements. For SERS studies, cells were seeded on round glass coverslips for a 70% final confluence. After cells were allowed to adhere overnight, the cells were incubated with NT-AuNPs diluted to the specified concentrations in complete DMEM for 24 h. NT-AuNP concentrations were specifically chosen to avoid toxicity or perturbing the cell cycle.[32]

Following nanoparticle incubation, single cells were irradiated for 2 h using the 785 nm diode laser at the indicated intensities. Time-dependent SERS spectra were recorded throughout the laser exposure to monitor the molecular changes upon photothermal heating of the NT-AuNPs. These spectra were collected from the area within the cell that displayed the most scattering due to nanoparticle localization, corresponding to the areas with the greatest enhancement of Raman vibrations from molecules in the nanoparticle microenvironment. The laser was directed into the microscope and focused on the sample by a 50×/0.75 N.A. objective, leading to a ∼1−2 μm spot size and resulting in single cell irradiation/resolution. For oven heating experiments, SERS spectra were obtained and averaged from 10 individual cells before and after heating. All SERS measurements were obtained in supplemented DMEM without phenol red. SERS spectra were measured in backscattering geometry using a 1200 lines/mm grating and collected by a CCD detector in the 400−1800 cm^{-1} range with a 10 s integration time. Spectra were background corrected using a cubic spline interpolation for the baseline fit by manually selecting points representative of the background. Dark-field images were collected using a Lumenera infinity2 CCD camera.

RESULTS AND DISCUSSION

Plasmonic photothermal therapy (PPT) is increasingly being investigated as a cancer therapy using gold nanoparticles (AuNPs) to absorb NIR light and rapidly produce heat, causing hyperthermia in the nanoparticle vicinity. However, differences in the size and shape of the nanoparticles lead to different absorption and scattering properties,[8,9] impacting the amount of heat generated and influencing the mechanism of cell death. Active nanoparticle targeting with proteins or cell-penetrating peptides (CPPs) and passive-targeting through the EPR effect results in nanoparticle accumulation (and therefore heat generation) either within individual cells, or within the tumor microenvironment, respectively. For this study, we have used actively targeted AuNPs due to their strong absorption properties leading to PPT-induced cell death, and their intense plasmonic field, allowing the monitoring of the SERS spectra for biochemical changes of the nanoparticle environment throughout the laser treatment and accompanying cell death.

Nearly spherical AuNPs were synthesized following the Turkevich/Frens citrate reduction method, where the gold salt precursor is reduced via sodium citrate, which also acts as the capping agent to complete nanocrystal growth. The AuNPs were characterized by TEM (Figure 1B) and found to have a

DOI: 10.1021/jacs.5b10997
J. Am. Chem. Soc. 2016, 138, 1258−1264

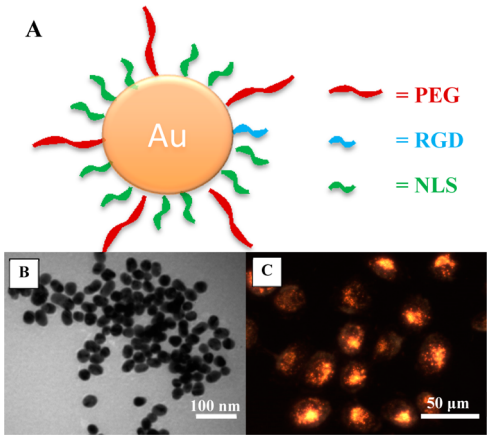

Figure 1. (A) Schematic showing nuclear-targeted AuNPs (NT-AuNPs) used in this study. (B) TEM micrograph of 29 nm citrate stabilized AuNPs. (C) Dark-field image of HSC-3 cells incubated with NT-AuNPs, showing the nanoparticles primarily localized at the perinuclear region.

~29 ± 3 nm diameter and an LSPR peak at 529 nm. The citrate-capped AuNPs were then conjugated with mPEG-SH to increase their stability and biocompatibility, and with RGD and NLS peptides, to promote cellular uptake[33] and localization at the nuclear region,[34] respectively. Successful conjugation is evident in the red-shift of the plasmon peak to longer wavelengths, from 529 nm for the as-synthesized AuNPs to 531 nm for PEG-AuNPs, and finally to 533 nm for the NT-AuNPs (Figure S1A). Cancer cells were then incubated with NT-AuNPs for 24 h to allow for uptake into the cells and localization at the nuclear region, which was confirmed through dark-field microscopy (Figure 1C). Localization of the AuNPs was critical, as it has been widely shown that having multiple AuNPs in close proximity shifts the observed LSPR peak to longer wavelengths due to coupling of their plasmonic fields.[10,35,36] This plasmonic coupling allows for the overlap with the 785 nm laser used for PPT heating and SERS measurements in this study. The AuNP treatment concentration (0.2 nM) was specifically chosen to allow for significant heat generation, resulting in PPT-induced cell death, while simultaneously monitoring the SERS spectra to identify the biochemical changes resulting from PPT. Following AuNP incubation, SERS spectra were collected from single cells for 2 h during continuous laser irradiation, leading to significant biochemical changes observed in the spectra and eventual cell death.

Initially, SERS bands appeared at ~500 and 654 cm^{-1} (Figure 2) primarily corresponding to −S−S− and −C−S− vibrations, respectively, from sulfur containing amino acids in proteins surrounding the AuNPs.[37,38] During 6.2 mW laser exposure, the −S−S− band disappeared almost entirely, indicating the likely rupture of disulfide bonds,[39] a critical component of protein structure, around the AuNPs due to PPT heating. By comparison, the intensity of the −C−S− vibration band remained relatively unchanged, indicating the continued presence of sulfur containing amino acids in the AuNP microenvironment. The slight changes in −C−S− vibration

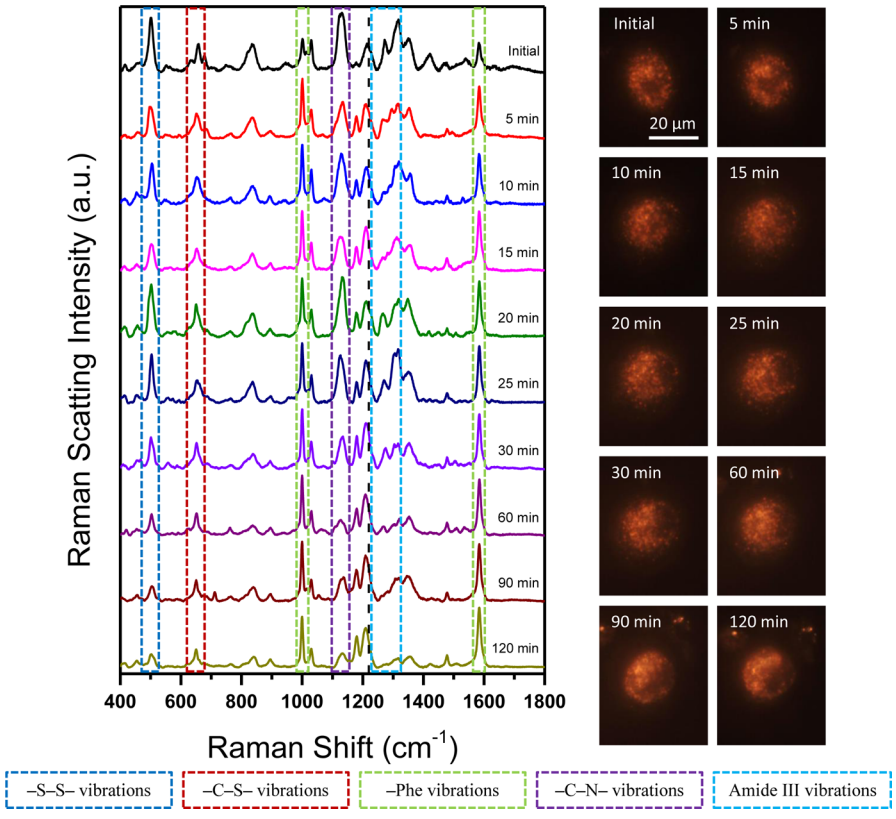

Figure 2. Time-dependent SERS spectra collected from a single HSC-3 cell during PPT cell death induced by continuous laser exposure at lower power (6.2 mW). The vertical line at 1225 cm^{-1} serves as a visual guide to highlight the shift in this vibrational peak from the amide III β-confirmation at 1225 cm^{-1} to the aromatic amino acid residue peaks at 1209 cm^{-1}, which in conjunction with the disappearance of additional vibrations around 500 cm^{-1} and in the 1250−1350 cm^{-1} range signals cell death. Corresponding dark-field images for each spectrum are also shown.

DOI: 10.1021/jacs.5b10997
J. Am. Chem. Soc. 2016, 138, 1258−1264

intensity could potentially be attributed to fluctuations in the interactions of the sulfur containing amino acids and the AuNP plasmonic field, and modifications in their dihedral angles as the amino acids would be more flexible following the loss of protein tertiary structure.[37,40]

Additionally, the Raman band observed at 1225 cm^{-1} in the initial spectra is mainly attributed to the amide III vibration of the β-sheet conformation of the proteins.[41,42] Upon laser exposure, this band shifted toward 1209 cm^{-1}, which is primarily due to the C_6H_5−C stretch of phenylalanine (with some contribution from tyrosine).[43] This was accompanied by the enhancement of the intensity of the 1180, 1001, and 1584 cm^{-1} bands, which are attributed to the in-plane CH bend,[43−45] ring breathing,[43,44,46] and in-plane CH stretching vibrations corresponding to phenylalanine moieties,[43,44,47] respectively. While fairly weak in the initial SERS spectra, these bands were seen to grow progressively stronger in intensity, eventually dominating the spectra along with the 1209 cm^{-1} vibration. Furthermore, additional spectral bands were seen at ∼835 cm^{-1} due to symmetric lipid−O−C−C−N stretches and tyrosine,[48,49] and at 1130 cm^{-1}, due to lipid *trans*-confirmations and the C−N backbone of proteins,[50−52] respectively. Additional vibrations are also observed in the 1275−1350 cm^{-1} region, attributed to the amide III vibrations of α-helix and random coil structures in the surrounding proteins,[52−54] as well as the $-CH_2$ twist in lipids.[49,52,55] Upon PPT heating, these protein and lipid structural vibrations disappeared, further supporting the hypothesis that, during laser exposure, actively targeted AuNPs generate intense amounts of local heat within the cell, disrupting lipid and protein structure and ultimately resulting in hyperthermia-induced cell death. Since the targeting peptides conjugated to the AuNPs do not contain phenylalanine, tryptophan, or tyrosine, the observed spectral features must originate from proteins within the cells. A detailed assignment of these spectral bands can be found in Table 1.

These spectral changes suggest a clear modification in protein confirmation within the cells during PPT heating. It is likely that the local heat induced by the plasmonic excitation could perturb/denature the conformation of the protein corona around the nanoparticles as well as in their surrounding microenvironment so as to expose the hydrophobic amino acid residues to the nanoparticle plasmonic field.[56] The appearance of Raman vibrations mainly corresponding to phenylalanine after laser exposure (beginning around 5 min and steadily increasing) strongly supports this hypothesis. Combined with the reduction in the intensity of vibrations corresponding to the disulfide (−S−S−) bonds appearing around 500 cm^{-1}, these features suggest rupturing of the disulfide bonds induced by the plasmonic heating. This is further support for protein denaturation in the AuNP microenvironment as these aromatic amino acids are highly hydrophobic and generally found buried within proteins,[57] shielding them from solvent exposure and, accordingly, from the plasmon field of the hydrophilic AuNPs.

The spectral changes resulting from PPT cell death noted above are seen in cells treated with 0.20 nM NT-AuNPs and exposed to the laser operating at both 6.2 mW (Figure 2) and 9.4 mW (Figure 3) intensity. While the initial and final spectra are similar in both cases, exposure to a higher laser intensity resulted in faster loss of protein structure, evident in the more rapid loss of the disulfide peak at ∼500 cm^{-1}, the exposure of phenylalanine residues at 1001 cm^{-1}, and the increase in amide III β-sheet vibration (along with Phe, Tyr, and lipid contributions) in the 1200−1220 cm^{-1} region, relative to the amide III α-helix vibrations in the 1275−1300 cm^{-1} region (Figure 4). These ratios illustrate the drastic changes that occur during PPT-induced cell death. With more intense laser exposure, these changes began immediately and occurred rapidly, following an exponential trend. This implies that, at high enough laser intensity (9.4 mW), protein and lipid structural features begin to denature upon laser exposure. However, at the intermediate intensity (6.2 mW), an induction period was observed. Initially, the structural changes occur very slowly, but begin to increase over time, following a sigmoidal trend commonly observed in dose response studies. This implies that, at this intermediate laser intensity, heat is generated slightly faster than it dissipates, leading to a slower but increasing rate of protein denaturation, while at higher intensity, these changes occur immediately.

Additionally, at lower laser intensity (2.6 mW, Figure S2) or lower NT-AuNP concentration with higher laser intensity (0.10 nM, 9.4 mW, Figure S3), these spectral changes were not observed, and the ratios in Figure 4 remain relatively unchanged. This indicates that there is a critical threshold of nanoparticle concentration and laser intensity (i.e., of heat) necessary to generate PPT-induced cell death. Below this threshold, heat is most likely dissipated more rapidly than it is generated, and no major spectral changes or cell death is observed. However, when the laser intensity and nanoparticle concentration are above this threshold, heat generation outpaces heat dissipation, which results in PPT-induced cell death. It should be noted that this critical threshold for cell death is likely dictated by the number of nanoparticles internalized within the cell and degree of localization, which depends on their surface chemistry and the AuNPs absorption properties, which are primarily dictated by the size, shape, and the degree of aggregation of the nanoparticles.

The same spectral changes arising from PPT-induced cell death can be observed by using smaller (15 nm) AuNPs modified with the same active-targeting ligands (NT-sAuNPs, see Figure S4 and Experimental Section in Supporting Information). Cell death is observed after incubation with 0.20 nM NT-sAuNPs upon exposure to both the lower (6.2 mW, Figure S5) and higher (9.4 mW, Figure S6) laser intensities previously observed to induce cell death in Figures 2

Table 1. Assignment of SERS Spectral Bands

shift (cm^{-1})	component	SERS band assignment
495−510	protein	−S−S−
640−660	protein	−C−S−
820−850	lipid and protein	lipid symmetric −O−C−C−N− stretch and Tyr
1000−1010	protein	Phe ring breathing
1020−1030	protein	Phe C−H in-plane bending and Trp ring breathing
1120−1140	lipid and protein	C−N backbone and Lipid *trans*-conformations
1170−1190	protein	C−H bend, C−C stretch, Tyr
1200−1210	protein	C_6H_5−C stretch of Phe and Tyr
1215−1225	protein	amide III (β-sheet)
1265−1300	protein	amide III (α-helix)
1300−1325	protein and lipid	$-CH_2$ twist
1440−1460	protein and lipid	$-CH_2$ bending (protein and lipid) and methylene deformation
1584−1592	protein	Phe

DOI: 10.1021/jacs.5b10997
J. Am. Chem. Soc. 2016, 138, 1258−1264

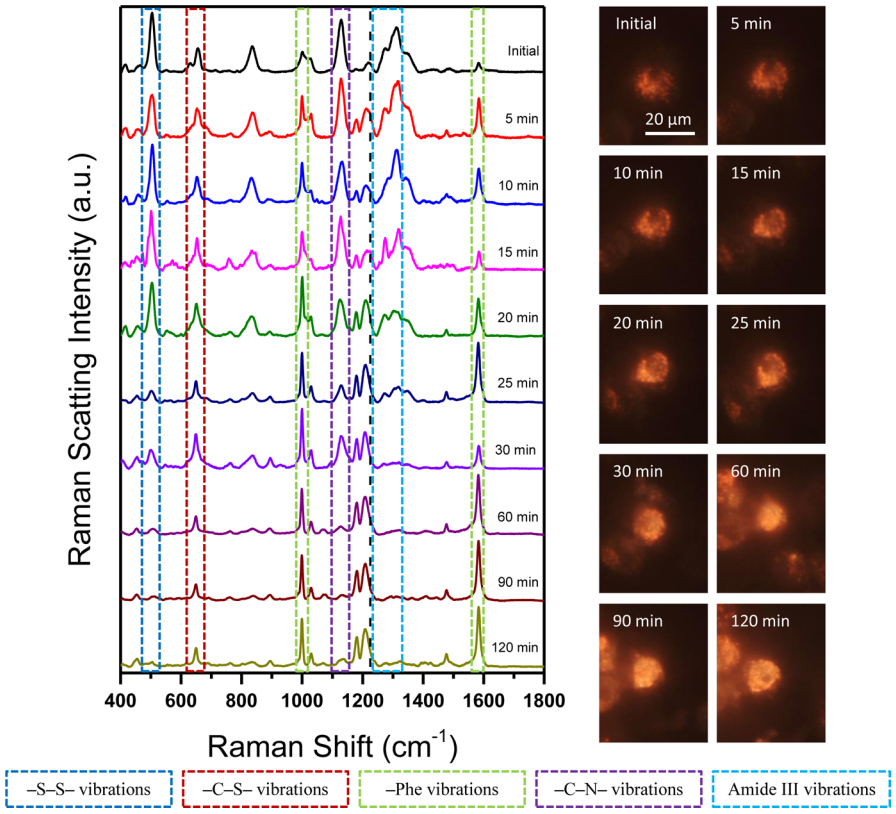

Figure 3. Time-dependent SERS spectra collected from a single HSC-3 cell during PPT cell death induced by continuous laser exposure at higher power (9.4 mW). The vertical line at 1225 cm^{-1} again serves as a visual guide to highlight the shift in this vibrational peak from the amide III β-confirmation to the aromatic amino acid residue peaks at 1209 cm^{-1}, which in conjunction with the disappearance of additional vibrations around 500 cm^{-1} and in the 1250 cm^{-1} – 1350 cm^{-1} range signals cell death. Corresponding dark-field images for each spectrum are also shown.

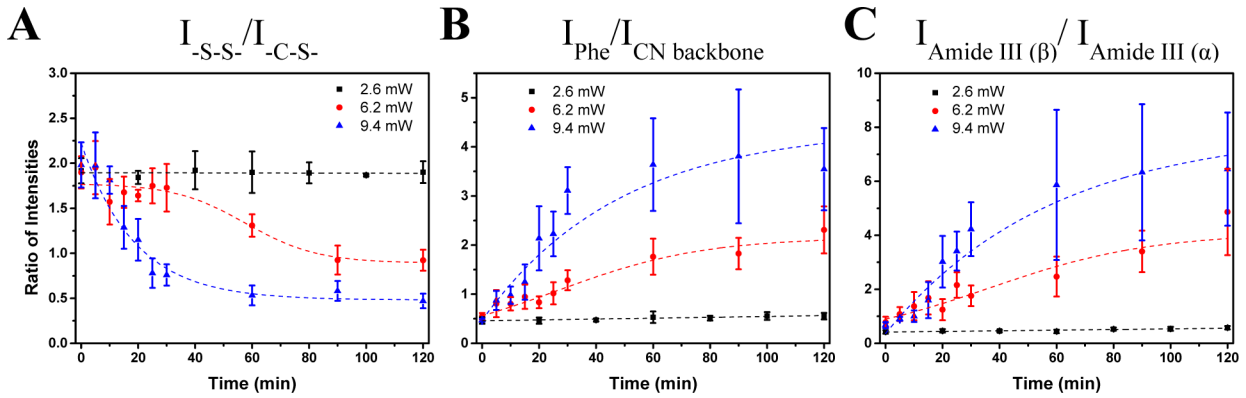

Figure 4. Plot showing changes in the SERS intensities for the ratio of the –S–S– and –C–S– vibrations (A), 1000 and 1130 cm^{-1} vibrations (B), and amide III β and α confirmations (C) during PPT heating at the indicated laser powers (n = 4 cells).

and 3 using the larger 30 nm AuNPs. The initial SERS spectra, as well as the final spectra after 120 min laser exposure, are nearly identical to those obtained using the larger NT-AuNPs. The same vibrational peaks are also observed to change throughout the PPT heating, including loss of the –S–S– vibration at ~500 cm^{-1}, the loss of protein and lipid structural features observed at 1130 cm^{-1} and in the 1275 cm^{-1} to 1350 cm^{-1} region, the shift of the 1225 cm^{-1} vibration due to amide III β-conformation in the initial spectra toward 1209 cm^{-1} vibration of phenylalanine, and the drastic increase in aromatic amino acid vibrational peaks at 1180, 1001, and 1584 cm^{-1}. The observation of the same spectral changes with different laser intensities and different nanoparticle sizes shows the reproducibility of this technique to induce and monitor PPT cell death with actively targeted AuNPs on the single cell level. This also supports the theory that there is a critical threshold of nanoparticle concentration and laser intensity (i.e., photothermal energy) necessary to induce cell death, which occurs through the denaturation of proteins and lipids in the nanoparticles' microenvironment. Moreover, using the highly focused laser of our Raman microscope results in single-cell irradiation and cell death without affecting adjacent cells, as can be clearly seen in Figure S7. After incubation with either the smaller or larger AuNPs, only the cell of interest displays the distinct morphological changes indicative of cell death, including cell shrinkage and increased light scattering.

DOI: 10.1021/jacs.5b10997
J. Am. Chem. Soc. 2016, 138, 1258–1264

Surrounding cells, some within a few microns of the cell being irradiated, appear unchanged even at the highest laser intensity used in this study, confirming the single cell specificity of our technique.

Additionally, cells were incubated with 0.10 nM NT-AuNPs, and SERS spectra were collected before (Figure 5A) and after

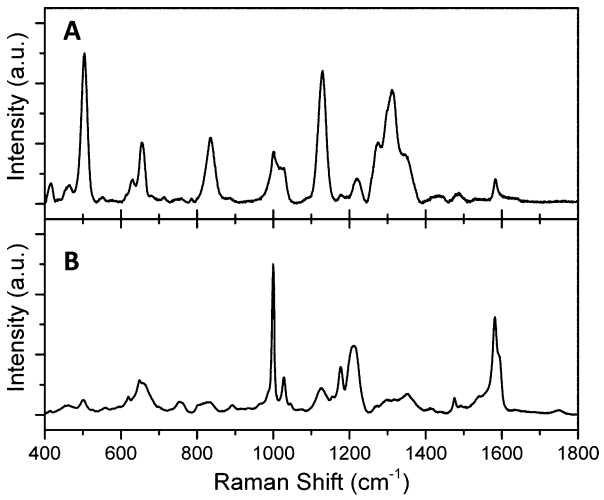

Figure 5. SERS spectra of HSC-3 cells incubated with 0.10 nM NT-AuNPs before (A) and after (B) oven heating at 100 °C for 7 min. The spectrum shown in part B is consistent with those shown in Figures 2 and 3, displaying characteristics attributed to cell death.

(Figure 5B) oven heating at 100 °C for 7 min. The initial spectra before oven heating were nearly identical to those obtained before PPT heating, highlighting the reproducibility of our technique across individual cells. The protein and lipid structural vibrations are again observed in the healthy cells before heating, with little contribution from the aromatic amino acid residue peaks. However, the structural vibrations of both proteins and lipids are no longer seen after oven heating, and the aromatic amino acid vibrations again dominate the SERS spectra, which were nearly identical to the final spectra obtained after PPT-induced cell death. To confirm cell death, we also performed flow cytometric analysis on cells incubated with 0.10 nM NT-AuNPs before (Figure S8A) and after oven heating (Figure S8B). A PI dye was used to tag necrotic cells, which have diminished membrane integrity, allowing the otherwise membrane impermeable dye to enter the necrotic cells. A FITC conjugated Annexin-V antibody was used to differentiate apoptotic cells due to its strong affinity for phosphatidylserine serine, a phospholipid found on the outer membrane of apoptotic cells. The HSC-3 cancer cells incubated with 0.10 nM NT-AuNPs were healthy before oven heating, exhibiting over 90% viability. After heating, over 95% of the cells were undergoing necrosis/late apoptosis, as evidenced by the large increase in fluorescence intensity from both the PI and FITC dyes, confirming cell death. The similarity between the SERS spectra of oven heated cells and the PPT treated cells, combined with the observed morphological changes in those cells, confirms the death of PPT treated cells.

CONCLUSION

We have used actively targeted AuNPs to induce PPT cell death upon laser exposure, and simultaneously monitor the corresponding molecular changes in real-time using SERS. We have found that continuous laser exposure of actively targeted nanoparticles internalized within cells leads to the modification of the protein and lipid structures, resulting in cell death. These alterations occur when the nanoparticle concentration/laser intensity (photothermal energy) reaches a minimum threshold. Above this critical point, cell death occurs through the same molecular changes, regardless of the nanoparticle size or laser intensity. It is important to note that cell death may still occur below this threshold, although not on the time scales studied herein. Additionally, the use of passively targeted nanoparticles would most likely result in different cell death mechanisms, as heat would be generated in the extracellular matrix surrounding the cell instead of from localized hotspots within it. Understanding the molecular mechanism of PPT cell death is crucial to understanding the treatment and optimizing its efficacy. We have presented a method to both induce and monitor this mechanism within single cells in real-time using actively targeted AuNPs.

ASSOCIATED CONTENT

Supporting Information

The Supporting Information is available free of charge on the ACS Publications website at DOI: 10.1021/jacs.5b10997.

UV−vis spectra and TEM images of AuNPs; detailed synthetic methods and characterization of smaller AuNPs, additional time-dependent SERS spectra obtained from cells treated with lower laser intensity, lower AuNP concentration, and smaller AuNPs; apoptosis-necrosis assay results for oven heated cells (PDF)

AUTHOR INFORMATION

Corresponding Author

*melsayed@gatech.edu.

Notes

The authors declare no competing financial interest.

ACKNOWLEDGMENTS

The authors wish to thank the support of the National Institutes of Health—National Cancer Institute under Grant No. U01CA151802. M.A. also wishes to acknowledge the support of the U.S. Department of Education GAANN fellowship. Sajanlal R. Panikkanvalappil and Steven M. Hira are thanked for helpful discussions.

REFERENCES

(1) Jain, P. K.; Huang, X. H.; El-Sayed, I. H.; El-Sayed, M. A. *Acc. Chem. Res.* **2008**, *41*, 1578.
(2) Dreaden, E. C.; Alkilany, A. M.; Huang, X. H.; Murphy, C. J.; El-Sayed, M. A. *Chem. Soc. Rev.* **2012**, *41*, 2740.
(3) Lane, L. A.; Qian, X.; Nie, S. *Chem. Rev.* **2015**, *115*, 10489.
(4) Yang, X.; Yang, M.; Pang, B.; Vara, M.; Xia, Y. *Chem. Rev.* **2015**, *115*, 10410.
(5) O'Brien, M. N.; Jones, M. R.; Brown, K. A.; Mirkin, C. A. *J. Am. Chem. Soc.* **2014**, *136*, 7603.
(6) Jain, R. K.; Stylianopoulos, T. *Nat. Rev. Clin. Oncol.* **2010**, *7*, 653.
(7) Link, S.; El-Sayed, M. A. *J. Phys. Chem. B* **1999**, *103*, 8410.
(8) Kelly, K. L.; Coronado, E.; Zhao, L. L.; Schatz, G. C. *J. Phys. Chem. B* **2003**, *107*, 668.
(9) Link, S.; El-Sayed, M. A. *Int. Rev. Phys. Chem.* **2000**, *19*, 409.
(10) Aioub, M.; Kang, B.; Mackey, M. A.; El-Sayed, M. A. *J. Phys. Chem. Lett.* **2014**, *5*, 2555.
(11) Kang, J. W.; So, P. T. C.; Dasari, R. R.; Lim, D. K. *Nano Lett.* **2015**, *15*, 1766.

DOI: 10.1021/jacs.5b10997
J. Am. Chem. Soc. 2016, 138, 1258−1264

(12) Meyers, J. D.; Cheng, Y.; Broome, A. M.; Agnes, R. S.; Schluchter, M. D.; Margevicius, S.; Wang, X. N.; Kenney, M. E.; Burda, C.; Basilion, J. P. *Part. Part. Syst. Char.* **2015**, *32*, 448.
(13) Dreaden, E. C.; Mwakwari, S. C.; Sodji, Q. H.; Oyelere, A. K.; El-Sayed, M. A. *Bioconjugate Chem.* **2009**, *20*, 2247.
(14) Dhar, S.; Daniel, W. L.; Giljohann, D. A.; Mirkin, C. A.; Lippard, S. J. *J. Am. Chem. Soc.* **2009**, *131*, 14652.
(15) Huang, X. H.; El-Sayed, I. H.; Qian, W.; El-Sayed, M. A. *J. Am. Chem. Soc.* **2006**, *128*, 2115.
(16) O'Neal, D. P.; Hirsch, L. R.; Halas, N. J.; Payne, J. D.; West, J. L. *Cancer Lett.* **2004**, *209*, 171.
(17) Perez-Hernandez, M.; del Pino, P.; Mitchell, S. G.; Moros, M.; Stepien, G.; Pelaz, B.; Parak, W. J.; Galvez, E. M.; Pardo, J.; de la Fuente, J. M. *ACS Nano* **2015**, *9*, 52.
(18) Albanese, A.; Tang, P. S.; Chan, W. C. W. *Annu. Rev. Biomed. Eng.* **2012**, *14*, 1.
(19) Perrault, S. D.; Walkey, C.; Jennings, T.; Fischer, H. C.; Chan, W. C. W. *Nano Lett.* **2009**, *9*, 1909.
(20) Ghosh, P.; Han, G.; De, M.; Kim, C. K.; Rotello, V. M. *Adv. Drug Delivery Rev.* **2008**, *60*, 1307.
(21) Huang, X. H.; Kang, B.; Qian, W.; Mackey, M. A.; Chen, P. C.; Oyelere, A. K.; El-Sayed, I. H.; El-Sayed, M. A. *J. Biomed. Opt.* **2010**, *15*, 058002.
(22) Lowery, A. R.; Gobin, A. M.; Day, E. S.; Halas, N. J.; West, J. L. *Int. J. Nanomed.* **2006**, *1*, 149.
(23) Rengan, A. K.; Bukhari, A. B.; Pradhan, A.; Malhotra, R.; Banerjee, R.; Srivastava, R.; De, A. *Nano Lett.* **2015**, *15*, 842.
(24) Burke, A. R.; Singh, R. N.; Carroll, D. L.; Wood, J. C. S.; D'Agostino, R. B.; Ajayan, P. M.; Torti, F. M.; Torti, S. V. *Biomaterials* **2012**, *33*, 2961.
(25) Chen, J. Y.; Glaus, C.; Laforest, R.; Zhang, Q.; Yang, M. X.; Gidding, M.; Welch, M. J.; Xia, Y. N. *Small* **2010**, *6*, 811.
(26) Tong, L.; Zhao, Y.; Huff, T. B.; Hansen, M. N.; Wei, A.; Cheng, J. X. *Adv. Mater.* **2007**, *19*, 3136.
(27) Kneipp, K.; Wang, Y.; Kneipp, H.; Perelman, L. T.; Itzkan, I.; Dasari, R.; Feld, M. S. *Phys. Rev. Lett.* **1997**, *78*, 1667.
(28) Nie, S. M.; Emory, S. R. *Science* **1997**, *275*, 1102.
(29) Turkevich, J.; Stevenson, P. C.; Hillier, J. *Discuss. Faraday Soc.* **1951**, *11*, 55.
(30) Frens, G. *Nature, Phys. Sci.* **1973**, *241*, 20.
(31) Xue, H.; Atakilit, A.; Zhu, W. M.; Li, X. W.; Ramos, D. M.; Pytela, R. *Biochem. Biophys. Res. Commun.* **2001**, *288*, 610.
(32) Aioub, M.; Austin, L. A.; El-Sayed, M. A. *J. Phys. Chem. Lett.* **2014**, *5*, 3514.
(33) Zitzmann, S.; Ehemann, V.; Schwab, M. *Cancer Res.* **2002**, *62*, 5139.
(34) Tkachenko, A. G.; Xie, H.; Liu, Y. L.; Coleman, D.; Ryan, J.; Glomm, W. R.; Shipton, M. K.; Franzen, S.; Feldheim, D. L. *Bioconjugate Chem.* **2004**, *15*, 482.
(35) Jain, P. K.; El-Sayed, M. A. *J. Phys. Chem. C* **2008**, *112*, 4954.
(36) Huang, D.; Byers, C. P.; Wang, L. Y.; Hoggard, A. L.; Hoener, B.; Dominguez-Medina, S.; Chen, S. S.; Chang, W. S.; Landes, C. F.; Link, S. *ACS Nano* **2015**, *9*, 7072.
(37) Vanwart, H. E.; Lewis, A.; Scheraga, H. A.; Saeva, F. D. *Proc. Natl. Acad. Sci. U. S. A.* **1973**, *70*, 2619.
(38) Vanwart, H. E.; Scheraga, H. A. *J. Phys. Chem.* **1976**, *80*, 1823.
(39) Kang, B.; Austin, L. A.; El-Sayed, M. A. *ACS Nano* **2014**, *8*, 4883.
(40) Ding, F.; Jha, R. K.; Dokholyan, N. V. *Structure* **2005**, *13*, 1047.
(41) Maiti, N. C.; Apetri, M. M.; Zagorski, M. G.; Carey, P. R.; Anderson, V. E. *J. Am. Chem. Soc.* **2004**, *126*, 2399.
(42) Panikkanvalappil, S. R.; Hira, S. M.; Mahmoud, M. A.; El-Sayed, M. A. *J. Am. Chem. Soc.* **2014**, *136*, 15961.
(43) Asher, S. A.; Johnson, C. R.; Ludwig, M. *Biophys. J.* **1986**, *49*, A331.
(44) Willets, K. A. *Anal. Bioanal. Chem.* **2009**, *394*, 85.
(45) Thomas, G. J. *Annu. Rev. Biophys. Biomol. Struct.* **1999**, *28*, 1.
(46) Wei, F.; Zhang, D. M.; Halas, N. J.; Hartgerink, J. D. *J. Phys. Chem. B* **2008**, *112*, 9158.
(47) Premasiri, W. R.; Lee, J. C.; Ziegler, L. D. *J. Phys. Chem. B* **2012**, *116*, 9376.
(48) Zheng, R.; Zheng, X. J.; Dong, J.; Carey, P. R. *Protein Sci.* **2004**, *13*, 1288.
(49) Wu, H. W.; Volponi, J. V.; Oliver, A. E.; Parikh, A. N.; Simmons, B. A.; Singh, S. *Proc. Natl. Acad. Sci. U. S. A.* **2011**, *108*, 3809.
(50) Puppels, G. J.; Demul, F. F. M.; Otto, C.; Greve, J.; Robertnicoud, M.; Arndtjovin, D. J.; Jovin, T. M. *Nature* **1990**, *347*, 301.
(51) Lippert, J. L.; Peticolas, W. L. *Proc. Natl. Acad. Sci. U. S. A.* **1971**, *68*, 1572.
(52) Premasiri, W. R.; Moir, D. T.; Klempner, M. S.; Krieger, N.; Jones, G.; Ziegler, L. D. *J. Phys. Chem. B* **2005**, *109*, 312.
(53) Asher, S. A.; Ianoul, A.; Mix, G.; Boyden, M. N.; Karnoup, A.; Diem, M.; Schweitzer-Stenner, R. *J. Am. Chem. Soc.* **2001**, *123*, 11775.
(54) Rygula, A.; Majzner, K.; Marzec, K. M.; Kaczor, A.; Pilarczyk, M.; Baranska, M. *J. Raman Spectrosc.* **2013**, *44*, 1061.
(55) Stone, N.; Kendall, C.; Smith, J.; Crow, P.; Barr, H. *Faraday Discuss.* **2004**, *126*, 141.
(56) Pustovalov, V. K.; Smetannikov, A. S.; Zharov, V. P. *Laser Phys. Lett.* **2008**, *5*, 775.
(57) Schlamadinger, D. E.; Gable, J. E.; Kim, J. E. *J. Phys. Chem. B* **2009**, *113*, 14769.

DOI: 10.1021/jacs.5b10997
J. Am. Chem. Soc. 2016, 138, 1258−1264